

VILNIUS UNIVERSITY  
CENTER FOR PHYSICAL SCIENCES AND TECHNOLOGY

JUOZAS ADAMONIS

TERAHERTZ OPTOELECTRONICS COMPONENTS OF SEMICONDUCTOR  
MATERIALS WITH DEEP DEFECTS

Summary of doctoral dissertation

Physical sciences, physics (02 P)

Vilnius, 2015

Doctoral dissertation was prepared in 2010 - 2015 at Center for Physical Sciences and Technology.

**Scientific supervisor** - prof. habil. dr. Arūnas Krotkus (Center for Physical Sciences and Technology, Physical Sciences, Physics - 02 P).

**Scientific advisor** - dr. Ramūnas Adomavičius (Center for Physical Sciences and Technology, Physical Sciences, Physics - 02 P).

**Joint council of defense of the doctoral thesis on Physical Sciences at Vilnius University:**

**Chairman** - Prof. habil. dr. Valdas Sirutkaitis (Vilnius University, Physical Sciences, Physics - 02 P).

**Members:**

Dr. Kęstutis Grigoras (Aalto University, Espoo, Finland, Physics - 02 P);

Habil. dr. Žilvinas Kancleris (Center for Physical Sciences and Technology, Physical Sciences, Physics - 02 P);

Dr. Tadas Malinauskas (Vilnius University, Physical Sciences, Physics - 02 P);

Dr. Kęstutis Regelskis (Center for Physical Sciences and Technology, Physical Sciences, Physics - 02 P).

The official defense of the dissertation will be held at 15:00 on the 18th of September, 2015, in room 2006 at the Center for Physical Sciences and Technology.

Address: A. Goštauto 11, LT - 01108, Vilnius, Lithuania.

The summary of doctoral dissertation has been distributed on the 18th of August, 2015.

The dissertation is available at Vilnius University Library, at the library of Center for Physical Sciences and Technology and at the official website of the Vilnius University:

[www.vu.lt/lt/naujienos/ivykiu-kalendorius](http://www.vu.lt/lt/naujienos/ivykiu-kalendorius).

VILNIAUS UNIVERSITETAS  
FIZINIŲ IR TECHNOLOGIJOS MOKSLŲ CENTRAS

JUOZAS ADAMONIS

OPTOELEKTRONINIAI TERAHERCINIO DAŽNIŲ DIAPAZONO KOMPONENTAI IŠ  
PUSLAIDININKIŲ SU GILIAIS CENTRAIS

Daktaro disertacijos santrauka

Fiziniai mokslai, fizika (02 P)

Vilnius, 2015

Disertacija rengta 2010 – 2015 metais Fizinių ir technologijos mokslų centro, Puslaidininkių fizikos institute, Optoelektronikos skyriuje, Ultrasparčios optoelektronikos laboratorijoje.

**Mokslinis vadovas** – prof. habil. dr. Arūnas Krotkus (Fizinių ir technologijos mokslų centras, fiziniai mokslai, fizika – 02 P).

**Mokslinis konsultantas** – dr. Ramūnas Adomavičius (Fizinių ir technologijos mokslų centras, fiziniai mokslai, fizika – 02 P).

**Disertacija ginama jungtinėje Vilniaus Universiteto Fizikos mokslų krypties taryboje:**

**Pirmininkas** – prof. habil. dr. Valdas Sirutkaitis (Vilniaus universitetas, fiziniai mokslai, fizika – 02 P).

**Nariai:**

Dr. Kęstutis Grigoras (Aalto universitetas, Espoo, Suomija, fiziniai mokslai, fizika – 02 P);

Habil. dr. Žilvinas Kancleris (Fizinių ir technologijų mokslų centras, fiziniai mokslai, fizika – 02 P);

Dr. Tadas Malinauskas (Vilniaus universitetas, fiziniai mokslai, fizika – 02 P);

Dr. Kęstutis Regelskis (Fizinių ir technologijos mokslų centras, fiziniai mokslai, fizika – 02 P).

Disertacija bus ginama viešame Fizikos mokslo krypties tarybos posėdyje 2015 m. rugsėjo 18 d. 15 val. Fizinių ir technologijos mokslų centre 206 auditorijoje.

Adresas: A. Goštauto 11, LT – 01108 Vilnius, Lietuva.

Disertacijos santrauka išsiųsta 2015 m. rugpjūčio 18 d.

Disertaciją galima peržiūrėti Vilniaus universiteto, Fizinių ir technologijos mokslų centro bibliotekose ir VU interneto svetainėje adresu: [www.vu.lt/lt/naujienos/ivykiu-kalendorius](http://www.vu.lt/lt/naujienos/ivykiu-kalendorius).

## Content

Introduction.....	6
Statements presented for defense: .....	9
Motivation.....	12
1 Photoconductivity measurements .....	13
1.1 Optical pump THz probe measurements.....	13
1.2 Picosecond photoconductivity measurements .....	16
1.3 Determination of defect parameters .....	17
2 THz generation .....	19
2.1 Investigation of optoelectronics components driven with the 1 $\mu\text{m}$ femtosecond laser .....	19
2.2 THz burst emission system with a diffraction grating optical stretcher .....	21
2.3 THz burst emission system based on the picosecond fiber laser .....	24
3 THz imaging .....	28
3.1 Coherent THz imaging.....	28
3.2 Incoherent imaging.....	29
Conclusions.....	32
Santrauka .....	34
Brief information about the author .....	36
Literature.....	37

## Introduction

From the practical point of view the THz radiation is very attractive because of phenomena that could be observed in this frequency range. A vast amount of non-polar molecules do not react to the THz field, while polar molecules such as H<sub>2</sub>O, N<sub>2</sub>, O<sub>2</sub>, CO, SO<sub>2</sub>, HCl etc. strongly interact with this field. Absorption spectra of various polar molecules have sufficient absorption peaks in the THz range originating from their rotational and vibrational states. These features are of interest in the case of the environment control, air pollution observation and gas detection. Besides, THz waves partly penetrate through clothing fabrics [1], polymers [2] or paper [3], which allows one to perform the THz imaging of objects, hidden behind these visually opaque materials. THz radiation has great potential in security as it can be used to detect hidden weapons. Drugs, plastic explosives and flammable liquids also have characteristic absorption peaks in the THz frequency domain. All this enables utilizing the aforementioned radiation for detection of these materials or ensuring safety in public gathering places.

Unfortunately, at the present time applications of THz systems are at the primary stage and they are still mostly used in the laboratory research. Semiconductor optoelectronic components and femtosecond lasers are widely employed in terahertz spectroscopy systems for spectroscopic measurements and THz imaging. Most commonly THz systems are activated with Ti:Sapphire lasers ( $\lambda = 800$  nm), whose photon energy quantum is slightly higher than the band gap of the GaAs crystal. Low temperature GaAs layers (LT GaAs) grown by means of molecular beam epitaxy have large defect concentrations, that act as electron traps. Other important features of these layers - large resistance, short carrier lifetime and high electron mobility - makes LT GaAs an attractive material for the THz component production. At present, both the LT GaAs and Ti:Sapphire laser technologies have reached a relatively mature level and their production is widely developed. Despite that, complex and bulky multi-stage optical pumping of Ti:Sapphire lasers limits a wider use of THz systems.

For generation and registration of THz radiation compact and potentially less expensive semiconductor and fiber lasers emitting in the near infrared region of 1  $\mu$ m and

1.55  $\mu\text{m}$  are being more increasingly used [4,5]. On the other hand, a large drawback of such systems is lack of efficient optoelectronic components operating in this wavelength range. Thus, in this work photoconductive antennas made from LT GaAs epitaxial layers were examined as THz emitters and detectors activated with the laser wavelength longer than the bandgap of the material ( $h\nu_0 < E_g$ ). In this case, photoconductivity of LT GaAs layers is governed by sole electrons excited from the defect band. This carrier generation mechanism is very attractive for THz photomixers, which were also investigated in this work. Finally, in this work a compact, easily and quickly tunable narrow linewidth THz pulse generation system, which was activated with the picosecond fiber laser, has been demonstrated. This system is simpler and more attractive for the THz imaging and environmental control applications.

**Main aims of the work are:**

- To investigate photoconductive antennas made of LT GaAs epitaxial layers as THz components activated with the long wavelength ( $h\nu_0 < E_g$ ) laser radiation.
- To develop and characterize a narrow spectral linewidth THz pulse generation system activated with the 1  $\mu\text{m}$  laser.

**Tasks:**

- To investigate photoelectric properties of photoconductive antennas made of LT GaAs epitaxial layers in the long wavelength range.
- To test photoconductive antennas made of LT GaAs layers as THz emitters, detectors and photomixers activated with the 1  $\mu\text{m}$  laser radiation.
- To characterize the THz burst system based on stretched femtosecond laser pulses.
- To develop, characterize and demonstrate applications of the fiber laser based terahertz burst system.

**Scientific novelty:**

- Picosecond photoconductivity spectra of LT GaAs and LT InGaAs epitaxial layers at the wavelength longer than a bandgap of these materials have been investigated.
- LT GaAs photoconductive antennas as THz photomixers activated with the 1  $\mu\text{m}$  laser radiation were tested.
- A narrow-band THz burst system activated with the picosecond fiber laser has been demonstrated and characterized.



### **Statements presented for defense:**

1. Picosecond photoconductivity spectra of photoconductive antennas, made from low-temperature grown GaAs and InGaAs epitaxial layers, store more information about initial electron distribution and were used for identification of a deep defect band position and a band-width of these materials.
2. It was found that GaAs epitaxial layers annealed at 420 °C temperature has an optimum defect concentration and electron mobility that result in the highest photosensitivity of these layers.
3. The THz burst generation system activated with picosecond fiber laser pulses is simpler, more compact and efficient than a system which uses a diffraction grating stretcher and femtosecond laser pulses.

### **List of publications related to the thesis:**

1. **J. Adamonis**, A. Arlauskas and A. Krotkus „Spectral measurements of picosecond photoconductivity in terahertz detectors made from low temperature grown GaAs and GaInAs“ *Phys Status Solidi A*, (2015).
2. **J. Adamonis**, N. Rusteika, R. Danilevičius and A. Krotkus „A Compact Terahertz Burst Emission System Driven With 1  $\mu\text{m}$  Fiber Laser“, *Opt. Comm. Vol. 293*, 61-64 (2013).
3. A. Bičiūnas, **J. Adamonis** and A. Krotkus „Terahertz time-domain-spectroscopy system using a 1 micron wavelength laser and photoconductive components made from low-temperature-grown“, *J. Infrared Milli. Terahz. Waves.*, 33(2), 183-191 (2012).

### **List of conference papers related to the thesis:**

1. **J. Adamonis**, R. Venckevicius, I. Kasalynas, R. Danilevicius, N. Rusteika, R. Adomavicius, and A. Krotkus, „Terahertz generation by optical mixing of chirped fiber laser pulses“, 39th International Conference on Infrared, Millimeter, and Terahertz waves (IRMMW-THz), Sep. 2014.
2. A. Arlauskas, **J. Adamonis**, R. Adomavicius, and A. Krotkus, „Excitation spectroscopy of terahertz emitters and detectors made from IIIIV semiconductors“, 38th

International Conference on Infrared, Millimeter, and Terahertz Waves (IRMMW-THz),  
Sep. 2013

3. I. Kašalynas, A. Švigelj, **J. Adamonis** et.al. „Performance of the antenna coupled microbolometers characterized by the quasi-optical measurements at frequencies 0.1-1.0 THz“ 38th International Conference on Infrared, Millimeter and Terahertz Waves (IRMMW-THz) 2013 Mainz on the Rhine, September 1st – 6th.
4. **J. Adamonis**, I. Kašalynas, N. Rusteika, R. Adomavičius ir A. Krotkus, „Terahercinių detektorių atsako dažninės priklausomybės nustatymas naudojant siaurajuosčius perderinamo dažnio terahercinius impulsus“ 40-oji Lietuvos nacionalinė fizikos konf., birželio 10 – 12 d., Vilnius, 2013.
5. A. Arlauskas, R. Adomavičius, **J. Adamonis**, A. Krotkus, „Spectral measurements of the picosecond photoconductivity in semiconductors by THz radiation pulses“, 3rd EOS Topical Meeting on Terahertz Science & Technology (TST 2012) 17 - 20 June 2012, Prague, Czech Republic.
6. **J. Adamonis**, N. Rusteika, R. Danilevičius, A. Krokus, „Terahertz generation by optical mixing of chirped fiber laser pulses“, „LO-2012“ 15th Int. Conf. on laser optics, 25-29 June 2012, St. Petersburg, Russia.
7. **J. Adamonis**, A. Bičiūnas, K. Bertulis, A. Krotkus, „Low-temperature-grown GaAs as a candidate for terahertz devices activated by 1  $\mu\text{m}$  wavelength laser pulses“, 13th Int. Conf.- School „Advanced Materials and Technologies“, 27–31 August 2011, Palanga, Lithuania.
8. **J. Adamonis**, A. Bičiūnas, K. Bertulis, A. Krotkus, „Ultrafast photoconductors from lowtemperature- grown GaAs for terahertz pulse generation and detection with femtosecond 1-  $\mu\text{m}$  wavelength laser pulses“, SIMC-XVI, 16th Semiconducting and Insulating Materials Conf., 19–23 June 2011, Stockholm, Sweden.
9. **J. Adamonis**, N. Rusteika, Y. Malevich, A. Krotkus, „Siaurajuostės terahercinės spinduliuotės generavimas su lazerine skaiduline pikosekundine čirpuotų impulsų sistema“, 39-oji Lietuvos nacionalinė fizikos konf., spalio 6 – 8 d., Vilnius, 2011.

**List of off-topic publications:**

1. R. Adomavičius, **J. Adamonis**, A. Bičiūnas, A. Krotkus, A. Atrashchenko, V. Evtikhiev, V. Ulin, M. Kaliteevski and R. Abram, „Terahertz pulse emission from nanostructured (311) surfaces of GaAs“, J. Infrared Milli. Terahz. Waves., 33(6), 599-604, 2012.
2. A. Bičiūnas, A. Arlauskas, **J. Adamonis**, P. Cicėnas, and A. Krotkus, „Physical mechanisms of terahertz pulse emission from photoexcited surfaces of tellurium crystals,“ Journal of Applied Physics, vol. 116, no. 9, p. 093102, Sep. 2014.

## Motivation

THz time domain spectroscopy (THz TDS) and photomixing using the continuous wave laser radiation are two different optoelectronic systems, which have already gained quite a mature level. However, the use of femtosecond lasers and complicated delay lines, which allow a real time signal registration, makes THz TDS an expensive and stationary system. Huge potential of the THz TDS system is attractive for many applications, but if one needs to perform one specific experiment this system might be too expensive. The THz photomixing scheme can supplement the aforementioned system in THz imaging experiments and spectroscopic measurements. In the case of THz imaging experiments, this system is superior to THz TDS, because there is no requirement to perform Fourier transformation. However, photomixing schemes usually consist of several DFB (distributed feedback) or DBR (distributed Bragg grating) continuous wave lasers, which require additional management. In such systems the generated THz frequency is selected by simply tuning the central wavelength of one of the lasers. Usually this is done by changing the laser temperature. D. H. Auston and A. S. Weling proposed the third type of a scheme, which combined both previously mentioned systems. A new system was generating THz pulses as in the THz TDS scheme, but these pulses were of a relatively narrow spectral width [6,7]. In the proposed system the laser beam intensity modulation was achieved with Michelson interferometer via mixing two chirped laser pulses. Great advantage of the system was its simple and fast frequency tuning, while wide femtosecond laser pulse spectra implied to achieve a tuning range wider than in continuous wave systems. However, a major disadvantage of such setup was a complex and bulky optical stretcher. In the present work, it was struggled to optimize this system by rearranging the above-mentioned optical component with chirped laser pulses emitted directly from a picosecond fiber laser. This scheme is potentially more compact and attractive for the applications under ambient conditions.

Most optoelectronic THz systems employ 800 nm and shorter wavelength laser radiation, and this choice is determined by the photosensitivity spectrum of LT GaAs - so far the most suitable material used for THz antenna manufacturing. There are

semiconductor and fiber lasers emitting at a longer wavelength, which are simpler, cheaper and can be used in optoelectronic THz systems. Unfortunately, the lack of photosensitive materials, which could be used for photoconductive antennas operating at a longer wavelength, deters from using such lasers. This is not so important for short THz pulse emitters, since narrow bandwidth semiconductors exposed to the laser illumination can generate sufficient THz radiation. On the other hand, the laser wavelength is of relevance to THz detectors and mixers. In this work, photoconductive antennas based on LT GaAs were investigated as THz detectors and photomixers activated with the longer wavelength laser radiation than the band-gap of the material.

## **1 Photoconductivity measurements**

### **1.1 Optical pump THz probe measurements**

The optical pump-THz probe experiment was performed on an as-grown LT GaAs layer on a SI GaAs substrate. The experimental curve corresponding to the LT GaAs layer showed fast dynamics immediately after the excitation with the laser pulse, but the shape of the transient was dominated by a slowly changing component. This component was also observed in the curve corresponding to the bare GaAs substrate and it was increasing linearly with the increase of the optical pump intensity. The slowly changing dynamics of the optically-induced THz absorption, obscuring the interpretation of pump-and-probe measurements, was probably caused by the electron excitation from various deep donor levels in the 600-  $\mu\text{m}$  thick SI GaAs wafer.

To eliminate the effect of the GaAs substrate, the same experiment was repeated on the LTG GaAs layer grown on a Bragg reflector substrate. Fig. 1 shows the shape of the optically induced THz absorption transient for an as-grown LT GaAs sample. As it can be seen, the introduction of the Bragg reflector into the structure has completely removed the slowly changing transient component as well as the constant background signal. The

FWHM duration of the induced THz absorption transient is  $\sim 0.9$  ps and its rise- and fall-

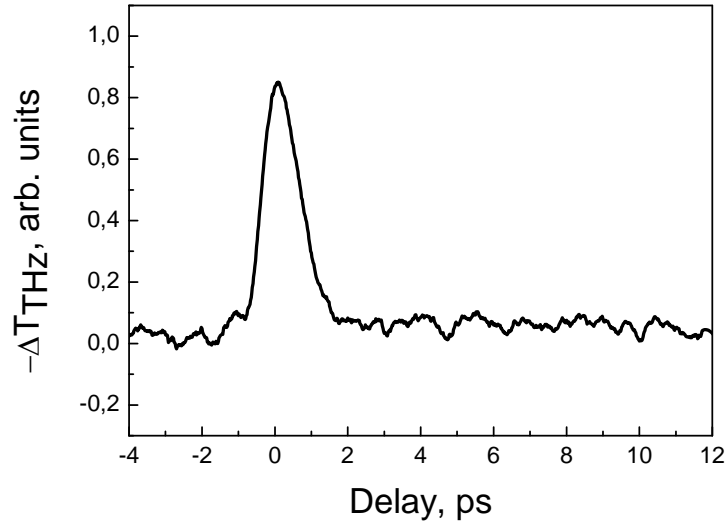


Fig. 1. Optically induced THz absorption transients measured for LT GaAs layer grown on a Bragg reflector.

times are similar. Thus, it can be concluded that the electron lifetime in the layer was shorter than the temporal resolution of the experiment determined by the duration of the THz pulses ( $\sim 0.8$  ps).

The induced THz absorption dependence on the near-infrared excitation level for

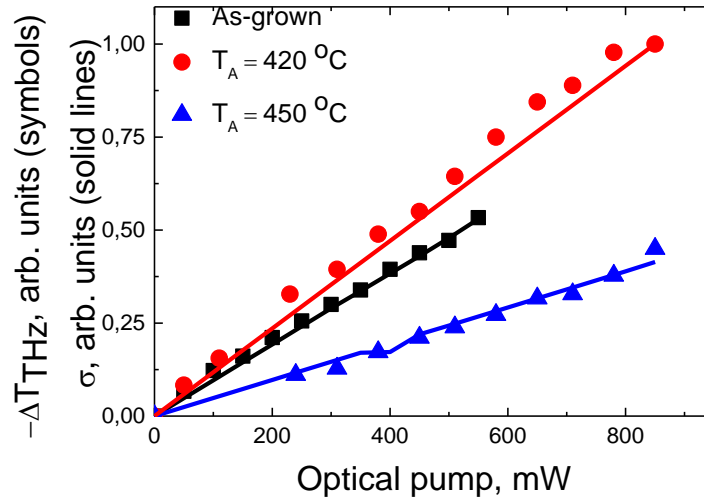


Fig. 2. Comparison of experimental and theoretical results. Points show experimental results of the THz transmittance peak value. Solid lines represent theoretical calculation of the charge transient peak value three samples was examined. The as-grown and annealed at 420 °C and 450 °C temperatures

LTG GaAs samples were grown on the Bragg reflector. The experimental dependence for the as-grown sample is shown in Fig. 2 and is signed by squares. The experimental curves corresponding to the samples annealed at 420 °C, 450 °C temperatures are also shown in Fig. 2 and are signed by circles and triangles, respectively. As it can be seen, THz absorption in all the studied samples increases linearly with the increment of the photoexcitation level. This fact provides strong evidence that in the as-grown and moderately annealed LTG GaAs, the photo-absorption at the 1  $\mu\text{m}$  wavelength is dominated by the electron transitions from the As-related defects rather than by two-photon or two-step absorption processes. The largest THz absorption signal was obtained from the sample annealed at 420 °C. It was slightly lower for the as-grown sample and approximately three times lower for the sample annealed at 450 °C.

To describe the excited charge density dependence on the optical excitation power rate equations based on the Shockley-Read-Hall model were solved. A nonlinear Riccati differential equation for the time dependent variable  $\Delta n$ , describing the concentration of photogenerated charge carriers, was obtained. This equation was solved numerically and the solution was compared to the results of the optical pump-THz probe experiment. Since the THz absorption is proportional to the photoconductivity of the sample, calculations were used to evaluate the excitation level dependence on the optical pump intensity. Following Ref. 8, the  $\text{As}_{\text{Ga}}$  defect concentrations ( $N_{\text{As}}$ ) for as-grown and annealed at 420 °C and 450 °C samples were assumed to be  $5 \times 10^{19} \text{ cm}^{-3}$ ,  $1 \times 10^{19} \text{ cm}^{-3}$  and  $2 \times 10^{18} \text{ cm}^{-3}$ , respectively. Due to the annealing the concentration of the  $\text{As}_{\text{Ga}}$  defects significantly decreased, so the electron mobility was expected to increase. Thus, in the calculations performed for both annealed samples, it was assumed that the electron mobility is 5 times larger than that for the as-grown sample. Similar results for the increment of the electron mobility were achieved by D. C. Look et al. [9]. The maximum charge excitation level corresponding to the non-equilibrium carrier density was evaluated to be  $\sim 1,9 \times 10^{15} \text{ cm}^{-3}$  for as-grown LT GaAs. This value is too low to observe the saturation of the defect-to-band transitions.

## 1.2 Picosecond photoconductivity measurements

Fig. 3 shows photoconductivity spectra of LT GaAs measured by using the monochromator light and the femtosecond pulse excitation. Both spectra show the presence

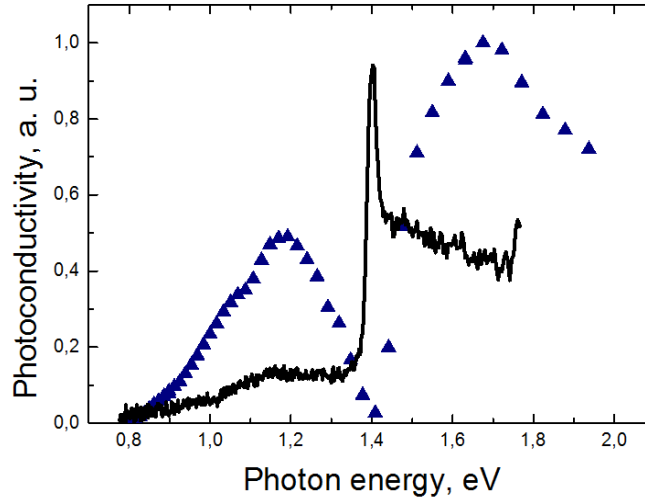


Fig. 3 Photoconductivity of the LTG GaAs sample measured under excitation with the femtosecond laser pulse (triangles) and constant excitation (solid line).

of a significant photoconductivity at photon energies lower than the optical absorption edge for GaAs of  $\sim 1.4$  eV. The origin of this sub-bandgap photoconductivity is most probably electron transitions from deep donor states typical of GaAs layers grown at a low-temperature by MBE. It has to be pointed out that the magnitude of picosecond photoconductivity in the LT GaAs sample increases with the increment of the photon energy reaching its maximum value at  $\lambda = 1 \mu\text{m}$ , which is only two times lower than at  $\lambda = 800$  nm corresponding to the central wavelength of the Ti:Sapphire laser spectrum. Further the decrement of picosecond photoconductivity is observed in the range between 1.2 and 1.4 eV. In this range photons have sufficient energy for the electron excitation from the defect band to the subsidiary valleys in the LT GaAs.

At larger photon energies ( $>1.4$  eV) the results of constant and pulsed illumination measurements are considerably different. The pulsed photoconductivity spectrum is monotonous up to the photon energy of  $h\nu \approx 1.7$  eV where the onset of photoexcited electron transitions to subsidiary low-mobility conduction band valleys occurs [10], whereas the photoconductivity measured by using the constant excitation in that spectral range



becomes very weak. Its peak observed in the vicinity of the energy bandgap is due to the photoconductance of the mobile and long living carriers excited in the thick substrate. The shape of the picosecond photoconductivity dependence on the photon energy is much more complex and possibly could be used for evaluating the energy position and other parameters of the deep defect levels. Such an evaluation based on the comparison of experimental and theoretical data will be presented in the next section.

### 1.3 Determination of defect parameters

The terahertz pulse emitter in our experiment was a p-type InAs crystal. At this material surface THz emission is caused by the nonlinear optical rectification [11,12]; electrical polarization of the crystal has its temporal dependence resembling the optical pulse envelope and its duration is  $\leq 200$  fs. A dipole antenna is distorting THz pulses incoming to the photoconductor, but their duration remains quite short - of the order of 0.5 ps. As this time is shorter than the electron energy relaxation time [13], the bias pulse will sample photoconductivity of the sample at the initial stages of electron dynamics after their excitation with femtosecond laser pulses.

In modeling the photoconductivity was calculated as a product of the photoexcited electron concentration and their mobility. As it was sampled in the experiments for the duration shorter than the electron energy relaxation time, a monoenergetic approximation [14] was used in modeling - all electrons were assumed to have the same energy constant in time and depending on the wavelength of photoexcitation. The experimentally measured long wavelength part of the picosecond photoconductivity spectrum of LTG GaAs is compared with the modeling results in Fig. 4. Parameters of the GaAs band structure were taken from [15]. The calculations taking into account different values of  $\varepsilon_{def}$  and  $\Delta\varepsilon_{def}$  are also presented. From this figure it can be seen that the shape of the defect-related photoconductivity band obtained from modeling is more sensitive to the value of  $\varepsilon_{def}$  than of  $\Delta\varepsilon_{def}$ . In the case of photoconductors made from LTG GaAs the best match between the experimental results and the simulation was achieved for  $\varepsilon_{def} = 0.77$  eV and  $\Delta\varepsilon_{def} = 78$  meV.

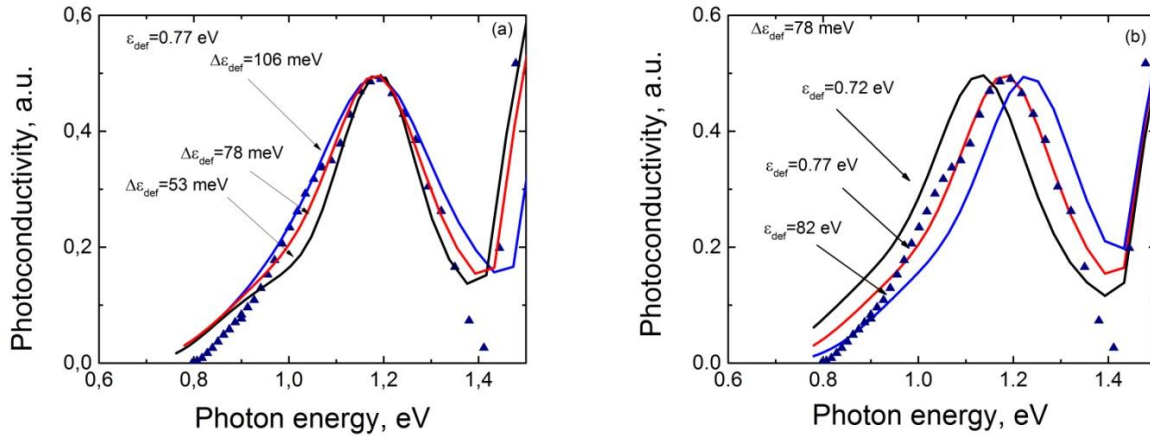


Fig. 4 Comparison of experimental (points) and calculated (lines) shapes of the photoconductivity corresponding to the defect band of LTG GaAs: a) various defect band positions; b) various defect band widths;

Experimental and theoretical picosecond photoconductivity spectra of LTG GaAs and LTG GaInAs in the whole investigated wavelength range are compared in Fig. 5 a and b. In the case of LT GaAs (Fig. 5 a), the coincidence between experimental and calculated spectra is quite good, especially when one takes into account that a rather rough theoretical model is used. Similar experiments and modeling were also performed with LT GaInAs

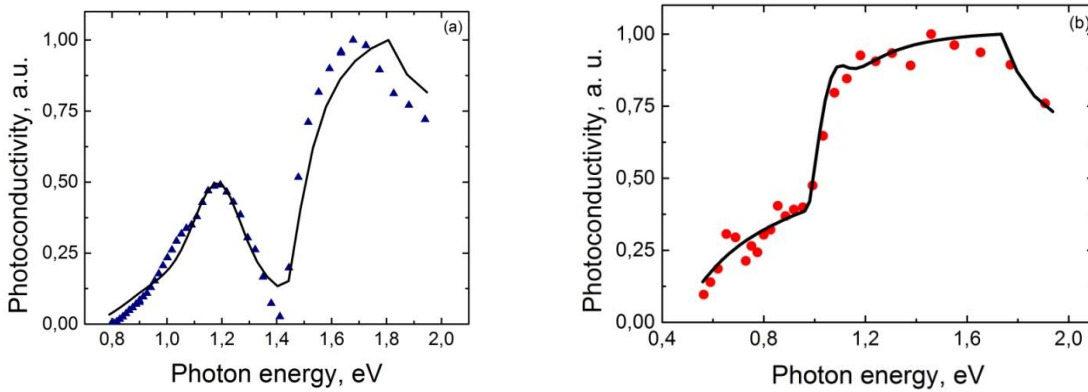


Fig. 5 Measured picosecond photoconductivity spectra (points) and their theoretical fits (lines) in: a) LT GaAs; b) LT GaInAs.

samples (Fig. 5 b). The coincidence between the experimental results and modeling in this case is even better than for LT GaAs. The sub-bandgap spectrum, related to the defect

photoconductivity part of the LT GaInAs, is observable quite clearly. The only difference from LT GaAs is that the maximum related to the onset of intervalley transfer is overlapping with the interband part of the spectrum. Fitting of the calculated results with the experimental data gives the defect band position in this material to be 0.4 eV with the bandwidth similar to LT GaAs and the  $\Gamma$ -L intervalley energy separation of 0.68 eV. It should be pointed out that in as-grown LT Ga<sub>0.7</sub>In<sub>0.3</sub>As a significant photoconductivity signal was observed at even longer wavelengths than in LT GaAs - the photosensitivity spectrum of this material was covering another technologically important spectral range of 1.5  $\mu\text{m}$ .

## 2 THz generation

### 2.1 Investigation of optoelectronics components driven with the 1 $\mu\text{m}$ femtosecond laser

In this section, photoconductive switches manufactured from the materials studied in the former experiment will be described. For comparison, in the experiments additional photoconductive switches made from LT GaAs annealed at 400 °C, 500 °C and higher temperatures were investigated. All the studied samples were grown without introduction of a Bragg reflector. All the switches were tested as the THz pulse emitters in the THz TDS system with the photoconductive detector made from the GaBiAs layer and illuminated with the average laser power of 20 mW for the THz pulse sampling. Experimental curves corresponding to the THz pulses emitted by these switches are shown in Fig. 6a. THz pulses emitted by the switches made from as-grown samples and annealed at 400 °C temperature were almost identical. The THz pulse with the largest amplitude was emitted by the device made from the layer annealed at the temperature of 420 °C (solid line) in Fig. 6a. For this layer, the optically induced THz absorption was also the largest, as it was shown in the previous section. Photoconductive antennas made from the as-grown and the annealed at

450 °C material emitted slightly lower-amplitude THz pulses. No THz pulses were detected from the devices annealed at 500 °C and higher temperatures.

In the second part of this experiment, the performance of GaBiAs detector was compared to the performance of a detector based on the LT GaAs which was annealed at 420 °C. The signal generated by the most efficient emitter (LT GaAs annealed at 420 °C) was detected with each of the detectors mentioned above. The Fourier-transform (FT) spectra of those signals are shown in Fig. 6 b. The FT spectrum of the signal detected with the GaBiAs detector (solid line) has a useful bandwidth reaching to 3 THz and its signal-to-noise ratio exceeds 50 dB. The FT spectrum corresponding to the photoconductive switch manufactured from the LTG GaAs (dashed line) is almost two times narrower and its sensitivity is ~15 times lower compared to the GaBiAs detector.

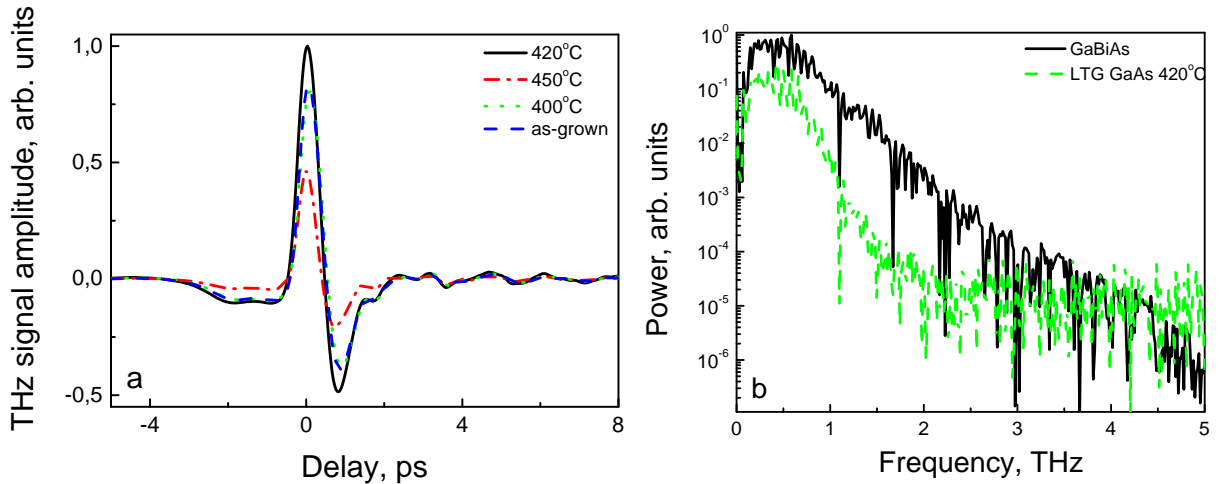


Fig. 6 THz pulses generated with photoconductive emitters made from as-grown and annealed at various temperatures LT GaAs epitaxial layers and sampled with the GaBiAs detector (a). Fourier spectrum of the THz pulse generated by LT GaAs photoconductor annealed at 420 °C and measured by the detectors made from the same material and from the epitaxial GaBiAs layer (b).

The most distinctive property of the photoconductive THz emitters, manufactured from LTG GaAs and annealed at moderate temperatures, is their high breakdown voltage. An alternating meander-shaped voltage waveform with the amplitude varying between -150 V and +150 V was applied to a 10 μm wide photoconducting gap. The dependence of the THz pulse amplitude generated by the device annealed at 420 °C on the bias voltage is shown in Fig. 7. The THz pulse amplitude increases linearly with the increasing voltage.

Thus, we can conclude that the electric breakdown field of the gap is larger than 150 kV/cm. This value is much higher than the value of the average electrical breakdown field of the

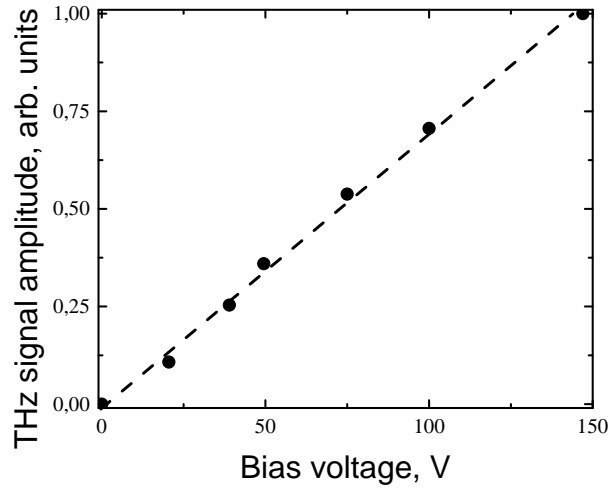


Fig. 7 Normalized THz signal amplitude generated by terahertz emitter, annealed at 420 °C, versus bias voltage.

LTG GaAs annealed at high temperatures, which is typically around 50 kV/cm [16]. A significant increase of this parameter for as-grown and annealed at lower temperatures devices could be explained by the influence of the hopping conduction. The hopping current prevents the nucleation of the high-field domain in the anode region and leads to a more homogeneous electrical field distribution along the band gap. Thus, the avalanche breakdown in the device occurs at higher voltage [16].

## 2.2 THz burst emission system with a diffraction grating optical stretcher

The THz burst system was characterized using LT GaAs and GaAsBi 24 photoconductive switches as THz photomixers. The excitation laser wavelength and stretched pulse duration were 1  $\mu\text{m}$  and  $\sim 41$  ps, respectively. The LT GaAs photomixer was biased with 70 V and excited with 70 mW average optical fluency. For GaAsBi photomixers these values were 50 V and 24 mW, respectively. A few THz transients measured with different photomixers are shown in Fig. 8 and Fig. 9.

Observed THz burst transients emitted by GaAsBi photoconductive switches are of an asymmetrical Gaussian shape. The acquired shape could be due to long recombination

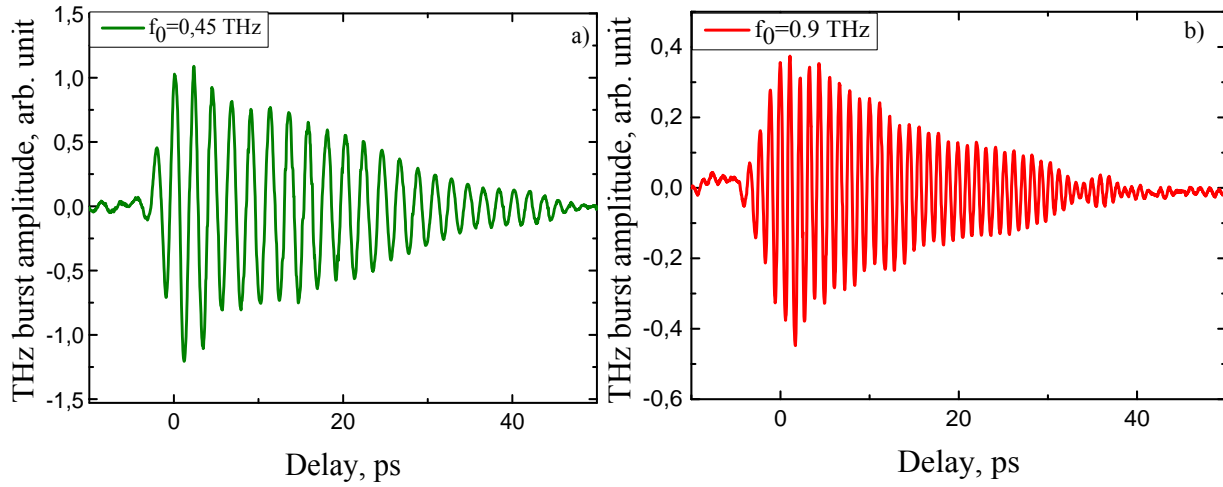


Fig. 8 GaAsBi photomixer THz burst transients with various frequencies.

time of charge carriers ( $t_{\text{rec}} = 2,3$  ps) in the emitter material. Besides, the shape of registered transients could have been governed by misalignment of Michelson interferometer

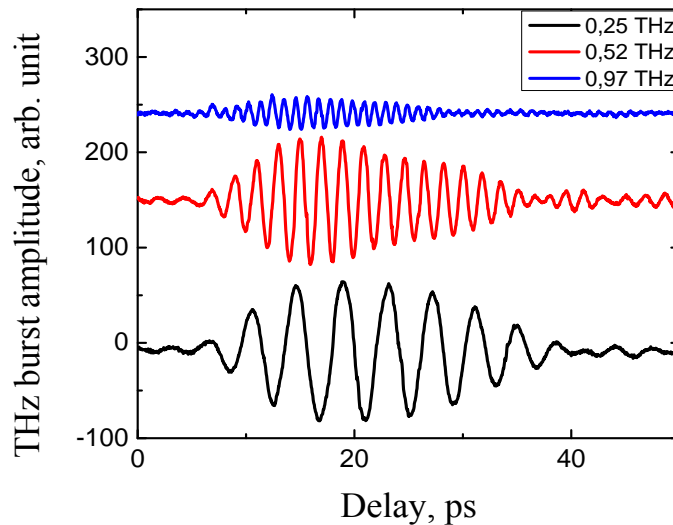


Fig. 9 LT GaAs photomixer THz burst transients with various frequencies.

branches. In this case, a better overlap would result in higher electric field oscillations. Fig. 9 exhibits a few different THz burst transients registered for the LT GaAs photomixer. In this case the observed bursts of THz pulses are of a more symmetrical shape. The measured THz frequency range of the system was similar to both types of photomixers. By changing

the delay between the chirped optical pulses from 1 to 6.3 ps THz transients ranging from 0.13 to 1 THz were registered. The frequency dependence on the delay between the pulses allowed determining the frequency chirp rate, which was evaluated to be  $\mu = 1.04 \text{ rad/ps}^2$ . Similar results were obtained from theoretical calculations  $\mu = 1.29 \text{ rad/ps}^2$ . The difference between those results could be explained by assuming that an additional pulse broadening is introduced while propagating through different optical components. A perfect match between experimental and theoretical results is obtained for the pulse duration of 130 fs, which in our case is a very plausible value.

Fig. 10 represents Fourier spectra of the transients measured at different delays between the chirped pulses. As it can be seen, THz burst spectra are up to 1 THz with their maximum situated at  $\sim 0.33 \text{ THz}$  and the signal to noise ratio of 40 dB. A rapid power decrement of the observed spectra most probably is due to the frequency cut off by resonant antennas of the emitter and the detector. Central frequency  $f_0$  dependence on the

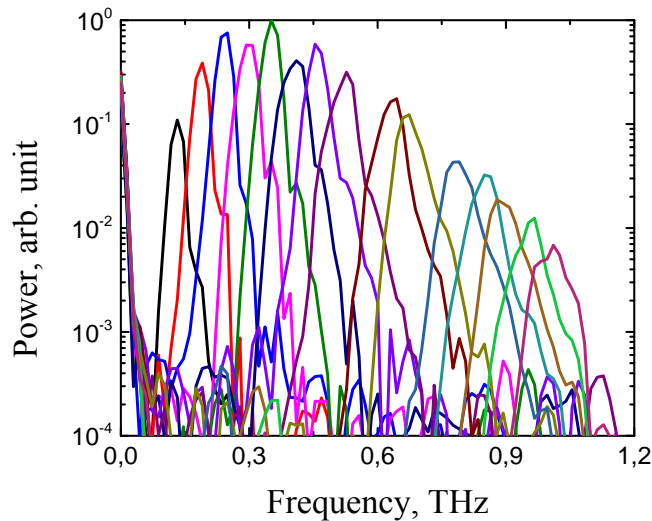


Fig. 10 FT spectra of different frequency THz bursts emitted by LT GaAs photomixer.

delay between the pulses  $\tau$  was determined from the THz burst spectra (see Fig. 11 a). As it could be expected frequency  $f_0$  exhibits a linear relation with the delay  $\tau$ . Fig. 11 b) illustrates the THz burst linewidth dependence on the central frequency  $f_0$ . In the frequency range from 0.13 to 1 THz the increment of the THz burst linewidth from  $\sim 44$  to  $\sim 125 \text{ GHz}$  is observed. The dotted line represents the THz burst width which would be if the third

order dispersion term  $\beta$  were zero. The difference between theoretical and experimental

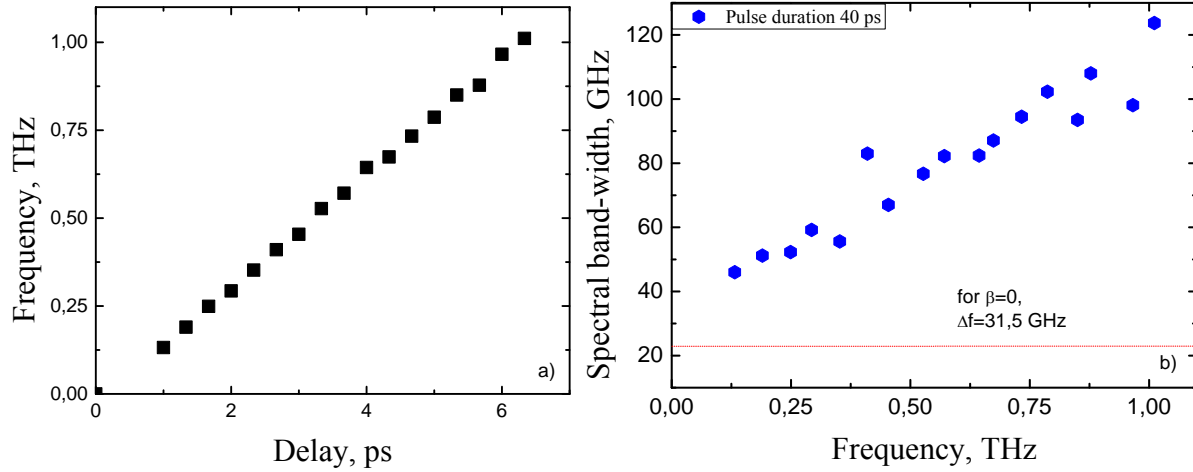


Fig. 11 THz burst a) frequency dependence on the delay between chirped pulses; b) linewidth dependence on the central frequency.

values implies that the third order dispersion term is sufficient in our experiment. This results in an increment of the THz burst bandwidth as well as a drop of the interference intensity. The  $\beta$  parameter in our case was evaluated to be  $1.52 \times 10^{-39}$  rad/ps<sup>3</sup>. This value is very close to that determined in the work of A. S. Weling [17], where authors evidenced a drop of the autocorrelation intensity due to the third order dispersion term. It can be concluded that the observed rapid decrement of the THz signal in Fig. 10 is determined not only by the resonant response of antenna but also by intensity decrement of interference of two chirped pulses.

### 2.3 THz burst emission system based on the picosecond fiber laser

Fig. 12 shows several THz transients generated and measured with ultrafast GaAsBi photoconductors activated by parts of the same optical pulse beating using the coherent homodyne detection technique. Varying the delay between the chirped pulse propagation in the interferometer arms from 0.8 ps to 4.5 ps, THz bursts with the frequencies ranging from 0.19 THz to 1 THz were produced. The chirp rate of the optical pulses of  $1.37$  rad/ps<sup>2</sup> was



evaluated from the experimentally determined linear THz burst frequency dependence on the delay between the chirped pulses.

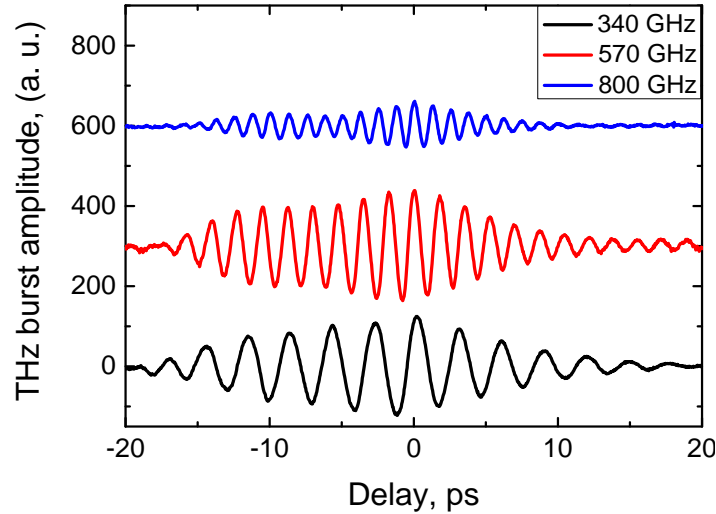


Fig. 12 THz burst transients with various frequencies.

Fig. 13 presents the Fourier spectra and full widths at half maximum (FWHM) of the transients measured at different delays between the chirped pulses. For the central frequency changing over the range from 0.19 to 1 THz, the frequency bandwidth of the transients increases only from 50 to 65 GHz. The coherent detection of the transients with larger central frequencies is not possible, most probably, due to too long carrier lifetime in the detecting antenna (about 1.5 ps) and the roll-off of the antenna gain characteristics in both photoconductive components. When measuring the absolute THz burst power dependence on the burst central frequency with the Golay cell (Fig. 14, black circles) the value of the roll-off frequency at which the power of the signal decreased to the  $1/e$  level was 1.1 THz and was much larger than the roll-off frequency evaluated from the coherent homodyne detection data ( $\sim 0.7$  THz). It is the evidence that system performance is mainly limited by the THz detector material and its antenna design characteristics. Absolute values of the average THz power, which are of the order of 9 nW at 0.3 THz are most probably also affected by the lack of the system optimization.

Due to the action of the group velocity dispersion (GVD) in fused silica the instantaneous frequencies are shifted in time following a linear law (linear chirp). However,

the third order dispersion term (TOD) and SPM introduce a nonlinearity of the chirp. It was previously shown that TOD was suppressing the interference of the optical pulses in the

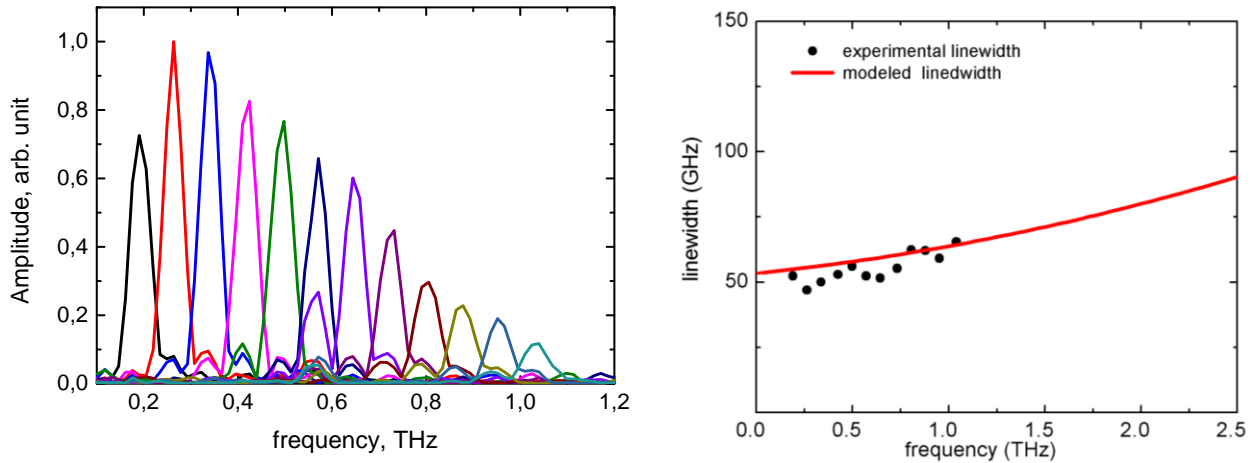


Fig. 13 FFT spectra of THz bursts at various frequencies (upper graph); FWHM of THz bursts spectra (dots) and theoretical evaluation (solid line) (lower graph).

Michelson interferometer [18] and increased the minimal obtainable linewidth, especially at higher frequencies [17]. Our method of producing THz radiation bursts is advantageous over the external femtosecond laser pulse stretching techniques because it gives a possibility to compensate some of nonlinear chirps induced by TOD with the opposite nonlinearity induced by SPM [19]. In this work, however, we only aimed to demonstrate the possibility of generating the THz field in the strong SPM regime and did not optimize the pulses for the best performance.

From the modeling of the propagation of the amplified pulses in the optical fiber was performed by solving the nonlinear Schrödinger equation using the symmetrized split step Fourier method [20]. Pulses from the oscillator were approximated with the Gaussian amplitude with the 5 ps duration to match the experimentally measured value. A simple point-like amplifier model was adopted and all the changes of the pulse duration and spectrum were assumed to take place in the passive fiber. The same pulse energy and the fiber length were used as in the experiment. Dispersion and nonlinearity of the fiber were taken from the literature. The agreement of the modeled and experimental spectra and the temporal pulse shape after the propagation in the fiber was very good.

We performed a simulation of a terahertz signal generated in a  $\chi^{(2)}$  nonlinear process using waveforms of the pulses from the modeling. Two chirped pulses of the same amplitude were delayed in time in respect of each other and overlapped in a nonlinear medium. The analytical evaluation in the case of the linear and third order dispersion (GVD and TOD) using the Gaussian pulse shape was performed in [17]. The resulting electrical

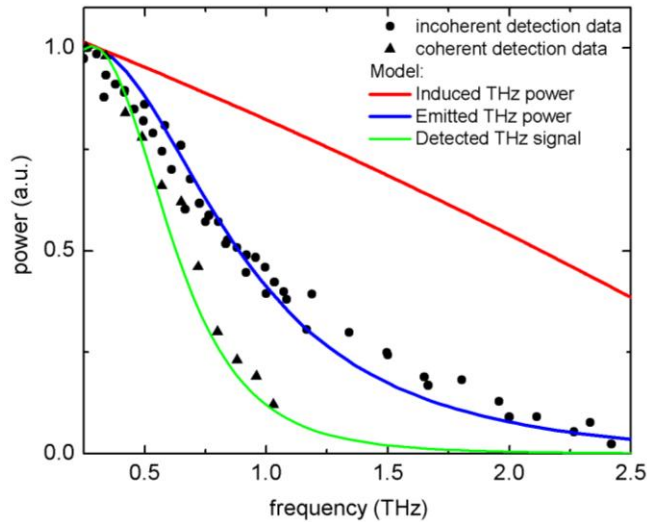


Fig. 14 THz burst power spectra from the coherent detection (triangles), incoherent detection (circles) and the modeling (lines).

field was modulated by the frequency corresponding to the instantaneous frequency difference between delayed chirped pulses, which varied almost linearly with the time delay. The linewidth of the spectrum was limited by TOD of the grating stretcher and was approximately 130 GHz at the 1 THz central frequency.

The results of our numerical simulations with the reconstructed pulses after the propagation through the optical fiber also showed the dependence close to linear central frequency on the delay between two pulses. The linewidth of the spectrum was in a good agreement with the experiment and was 63 GHz at the 1 THz central frequency (Fig. 13). The reduction of the linewidth in comparison to Ref. 6 was primarily attributed to lower TOD of the optical fiber compared to the grating stretcher and some non-linear chirp compensation by the SPM. The linewidth increases slowly with the central frequency. The simulated intensity of the THz signal decreases slowly when the central frequency is increased, reaching the  $1/e$  level at about 2.5 THz.

The difference between the bandwidth of the tunable THz signal by the coherent (0.7 THz) and incoherent (1.1 THz) measurements and obtained from the simulation (2.5 THz) is evident but could be expected from the following considerations. The THz spectrum measured with the Golay cell can be expressed as a product of the spectrum obtained from the difference frequency generation by optical mixing of two chirped pulses and the spectral response function of the emitter antenna, which was fitted with the resonance response function of the damped harmonic oscillator [21]. The difference frequency generation spectrum is determined by the optical pulse parameters and in our case it is quite flat (Fig. 14, red curve). The measured spectrum was fitted with the product of the modeled optical response and the resonance curve. The best fit (blue curve) corresponds to the central frequency  $\nu_0 = 0.3$  THz and Lorentzian linewidth  $\Gamma = 1.1$  THz. In the case of the coherent detection, the measured spectrum is also the product of the detector response function. In our case we assumed the same resonance curve as for the emitter. The resulting modeled signal (green) fits quite well the measured signal (black triangles) in the range of 0.2–1 THz where measurements were possible. It is also obvious that the main bandwidth limitation comes from the response of the antennas.

### **3 THz imaging**

#### **3.1 Coherent THz imaging**

The coherent THz imaging experiment was performed at the THz burst frequency  $f_0 = 0,75$  THz. A blade edge method was used to determine the diameter of THz radiation to be equal to  $\sim 1$  mm [22]. Fig. 15 represents results obtained from the THz imaging experiment. In general, a watermark picture is obtained by varying the thickness or density of the paper material. This property of the material results in an additional delay for THz radiation which is registered in our experiment. In the experiment a step of the XY stage was chosen to be 0.5 mm. For measurements of 10 litas watermark  $40 \times 20$  points and for 20



Fig. 15 THz images of watermarks of 10 and 20 litas performed at  $f_0 = 0,75$  THz.

litas  $40 \times 40$  points were registered, respectively. The recording time of one point was governed by the integration constant ( $t = 30$  ms) of a synchronous amplifier. On the other hand, the movement and stabilization of the XY delay line took around 1 s. As a result measurements of 10 litas lasted  $\sim 15$  min. and those of 20 litas — 30 min. From the acquired THz image pictures of both watermarks can be clearly seen.

### 3.2 Incoherent imaging

Firstly, the THz burst setup was tested as a characterization equipment for non-coherent THz detectors in the frequency range from 0.1 to 1 THz. For the test a microbolometer was selected as a sensing element. It was made of titanium, which was chosen among several appropriate materials, as its micromachining properties are suitable for the silicon processing technology. Dimensions of the microbolometer were  $12 \times 0.5$   $\mu\text{m}$ . The sensor was processed on the membrane of silicon nitride, and it was connected either to the double-dipole or to log-periodic type THz antenna.

The response dependence on the frequency of the antenna coupled Ti-based microbolometer detector was measured. The results are shown in Fig. 16. The response

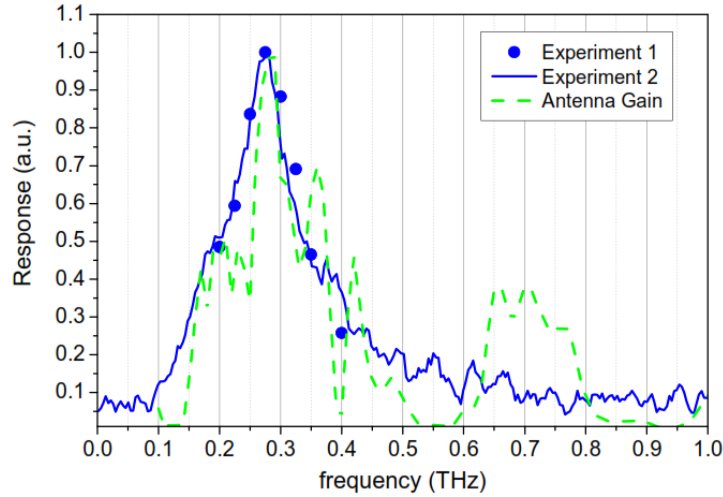


Fig. 16 Frequency response of the double-dipole-antenna-coupled microbolometer measured (Experiment 1) using selectively filtered photoconductive emitter radiation and (Experiment 2) by the system providing narrow band THz radiation bursts.

curve at maximum sensitivity values was measured the same with THz mixing and TDS experimental setups. The data demonstrated maximum sensitivity at frequency 275 GHz. Simulated gain of the microbolometer antenna is also presented in Fig. 16. Agreement between the first modeling data and the experiments is quite good.

Afterwards for the THz image acquisition of a few short response time, compact,

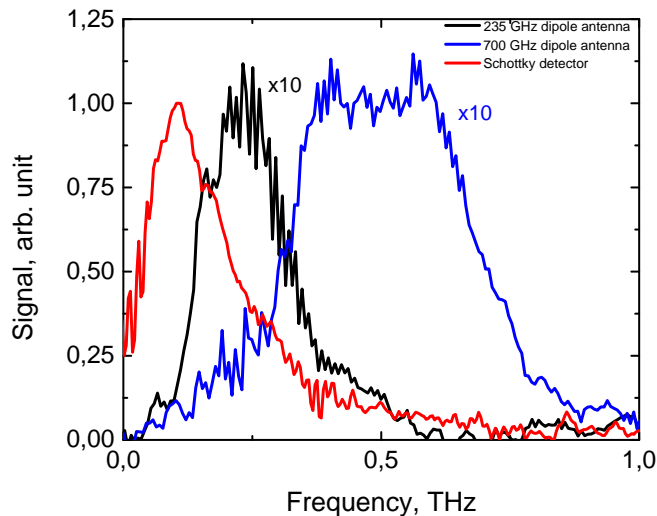


Fig. 17. Normalized signal spectrum of the dipole-antenna microbolometer optimized for different THz frequency detection (black and blue curves) and Schottky diode (red curves).

room temperature detectors were tested in operation with the THz burst system.

Commercially available antenna-coupled Ti-microbolometers [23-24] and zero-bias Schottky diodes were employed in the experiment. A microbolometer-based THz detectors with the double-dipole antenna designs possessed sensitivity of  $R_u \geq 300$  V/W and  $R_u \geq 50$  V/W with the noise-equivalent-power of  $NEP \leq 14$  pW/ $\sqrt{\text{Hz}}$  and  $NEP \leq 60$  pW/ $\sqrt{\text{Hz}}$  respectively. The NEP of the zero-bias Schottky diode was below 20 pW/ $\sqrt{\text{Hz}}$  at the measured 300 GHz frequency. The results for double-dipole and log-periodic antenna microbolometer detectors and zero-bias Schottky diode are shown in Fig. 17.

Further the fiber-laser-based THz emitter and the compact Schottky-based THz detector were taken to demonstrate application of such a system for the THz imaging. The THz image of explosive imitators in a plastic container was measured at the

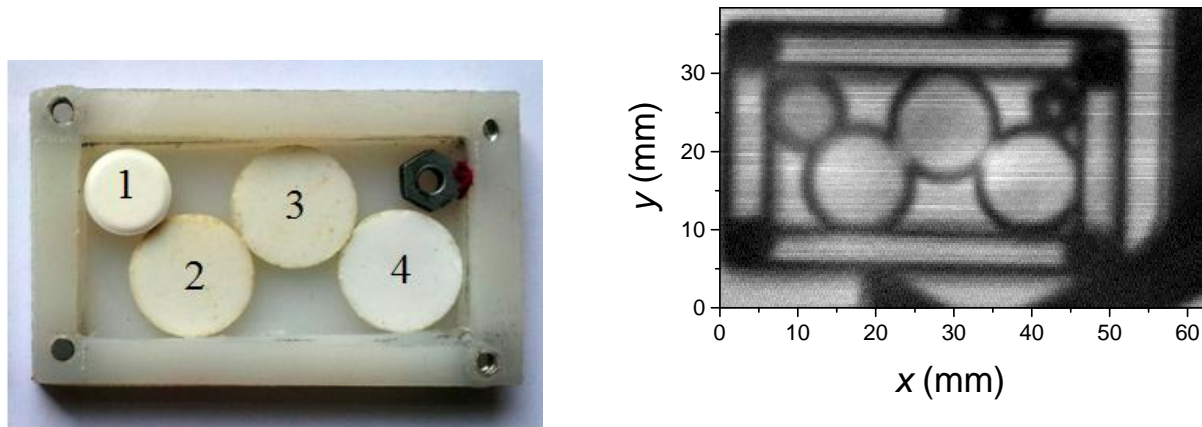


Fig. 18. THz image of drug pellets packed in plastic container measured using fiber-laser-based THz generator and antenna coupled Schottky-diode at 300 GHz frequency. Intensity scale is linear.

selected 300 GHz frequency (Fig. 18).

## Conclusions

1. Picosecond photoconductivity spectra of detectors made from epitaxial LT GaAs or  $\text{In}_{0.7}\text{Ga}_{0.3}\text{As}$  layers annealed at moderate temperatures, measured at laser wavelength longer than the material band-gap, are governed by the electron excitation from deep defects.
2. From the picosecond photoconductivity spectra of the LT GaAs and LT  $\text{In}_{0.7}\text{Ga}_{0.3}\text{As}$  optoelectronic switches, the energy position ( $\varepsilon_{\text{def}}$ ) and the band-width ( $\Delta\varepsilon_{\text{def}}$ ) of arsenic antisite defect bands in these materials were determined. Parameters obtained for LT GaAs epitaxial layers were  $\varepsilon_{\text{def}} = 0.77$  eV and  $\Delta\varepsilon_{\text{def}} = 78$  meV. For  $\text{In}_{0.7}\text{Ga}_{0.3}\text{As}$  these parameters were respectively  $\varepsilon_{\text{def}} = 0.4$  eV and  $\Delta\varepsilon_{\text{def}} = 70$  meV.
3. LT GaAs epitaxial layers annealed at 420 °C exhibit the highest photoconductivity when illuminated with the 1  $\mu\text{m}$  wavelength laser radiation. These layers are characterized by the electron capture time shorter than 1 ps. Aforementioned features make LT GaAs epitaxial layers annealed at 420 °C the best choice for THz components: emitters, detectors and photomixers activated with the 1  $\mu\text{m}$  wavelength laser radiation.
4. The electrical breakdown field in photoconductive antennas made from LT GaAs epitaxial layers, annealed at temperatures lower than 450 °C, the value of 150 kV/cm was determined. This value is greater than one achieved for pure GaAs crystals, because of the dominant hopping current, which prevents the high-field domain nucleation in the anode region and leads to a more homogeneous electrical field distribution along the band-gap.
5. The terahertz burst generation system pumped with solid-state femtosecond Yb:KGW laser pulses using two diffraction grating stretcher and LT GaAs photoconductive antenna as a THz photomixer was demonstrated. THz bursts reaching over 1 THz central frequency, up to 40 ps duration and spectral band-width of 40-120 GHz were generated with this system.
6. Picosecond fiber laser pumped terahertz bursts generation system was developed. With a use of a GaAsBi photomixer, electromagnetic pulses up to 2.5 THz were generated.



Spectral linewidth of THz burst was slightly increasing with the increment of frequency and at 1 THz was equal to 65 GHz.

7. In the THz imaging experiment the THz burst system tested in coherent and non-coherent detection modes. THz images were obtained in the range from 0.1 to 1 THz.

## Santrauka

Pirmoje šio darbo dalyje buvo koncentruotasi į paiešką naujų medžiagų tinkančių fotolaidžių THz emiterių, detektorių ir fotomaišiklių aktyvuojamų ilgabange (1 – 1,55  $\mu\text{m}$ ) lazerio spinduliuote gamybai. Atliekant optinio žadinimo THz zondavimo eksperimentą su ŽT GaAs sluoksniais užaugintais ant AlAs/GaAs Bragg'o veidrodžių ir atkaitintais vidutinėse temperatūrose, buvo iširta fotosužadintų elektronų dinamika. Parodyta, kad krūvininkų rekombinacijos trukmės šiuose sluoksniuose yra mažesnės už 1 ps, o indukuota THz impulsų sugertis didėja tiesiškai augant lazerio impulso intensyvumui. Didžiausia THz spinduliuotės sugertis stebėta sluoksniuose, kurių atkaitinimo temperatūra yra 420 °C. Šioje temperatūroje atkaitinti ŽT GaAs epitaksiniai sluoksniai, dėl optimalių pakeistinių arseno defektų koncentracijos ir elektronų judrio, pasižymi didžiausiu fotolaidumu, juos apšviečiant 1  $\mu\text{m}$  bangos ilgio lazerio spinduliuote. Tad 420 °C temperatūroje atkaitinti sluoksniai yra tinkamiausi THz komponentų: emiterių, detektorių ir maišiklių, aktyvuojamų 1  $\mu\text{m}$  bangos ilgio spinduliuote, gamybai.

Antroje darbo dalyje buvo išmatuotos THz detektorių fotolaidumo priklausomybės nuo aktyvuojančio femtosekundinio lazerio impulso bangos ilgio. Rasta, kad detektorių, pagamintų iš vidutinėse temperatūrose atkaitintų ŽT GaAs ir ŽT  $\text{In}_{0.7}\text{Ga}_{0.3}\text{As}$  epitaksinių sluoksnių, fotosužadavimo spektruose egzistuoja elektronų šuolių iš gilių defektų lygių sąlygota sugertis ilgesniuose už medžiagos sugerties kraštą bangos ilgiuose. Lyginant išmatuotus pikosekundinio fotolaidumo ŽT GaAs ir ŽT  $\text{In}_{0.7}\text{Ga}_{0.3}\text{As}$  fotovaržų spektrus su teoriniu modeliu, nustatytos arseno pakeistinių atomų juostų energetinės padėtys ir pločiai. Šie parametrai ŽT GaAs atveju buvo lygūs  $\epsilon_{\text{def}} = 0,77$  eV ir  $\Delta\epsilon_{\text{def}} = 78$  meV, o ŽT  $\text{In}_{0.7}\text{Ga}_{0.3}\text{As}$  atveju, atitinkamai  $\epsilon_{\text{def}} = 0,4$  eV ir  $\Delta\epsilon_{\text{def}} = 70$  meV.

Galiausiai, šiame darbe buvo pademonstruota THz pliūpsnių generavimo sistema, kaupinama femtosekundiniais kietakūnio Yb:KGW lazerio impulsais, naudojanti išorinį dviejų gardelių plėstuvą bei iš ŽT GaAs pagamintą fotolaidų optinių signalų maišytuvą. Tirta sistema generavo 40 ps trukmės, 40–120 GHz spektrinio pločio THz spinduliuotės pliūpsnius, kurių dažnis siekė 1 THz. Parodyta, kad THz pliūpsnių generavimo sistema, kaupinama skaidulinio pikosekundinio lazerio spinduliuote, yra kompaktiškesnė ir

patrauklesnė taikymams lauko sąlygomis už jos atitikmenį, naudojanči femtosekundinius lazerio impulsus bei išorinį dviejų gardelių plėstuvą. THz pliūpsnius generuojanti sistema buvo panaudota THz vaizdų sudarymui, koherentiniu ir nekoherentinio signalo registravimo būdais; dažnių srityje nuo 0,1 THz iki 1 THz gauti įvairių objektų vaizdai.

## Brief information about the author

**Name:** Juozas  
**Surname:** Adamonis  
**Date of birth:** March 24, 1985  
**Place of birth:** Vilnius, Lithuania  
**e-mail:** juozas.adamonis@ftmc.lt

### Education:

2004: Vilnius Žirmūnų gymnasium  
2008: Vilnius University – Bachelor’s degree in  
Telecommunication Physics and electronics  
2010: Vilnius University – Master’s degree in Optoelectronics  
2010 - 2014: PhD studies in Center for Physical Sciences and Technology

### Scientific experience:

2007 - 2010 engineer, Semiconductor Physics institute, Vilnius  
2010 - 2014 engineer, Center for Physical Sciences and Technology  
2015 - now junior scientific researcher, Center for Physical Sciences and  
Technology

### Specialization:

Ultrafast optoelectronics, THz generation, THz photomixing.

## Literature

- 
- [1] J. E. Bjarnason, T. L. J. Chan, A. W. M. Lee, M. A. Celis, and E. R. Brown, *Appl. Phys. Lett.* **85**(4), 519 (2004).
- [2] B. B. Hu and M. C. Nuss, *Optics Letters* **20**(16), 1716 (1995).
- [3] K. Kawase, Y. Ogawa, Y. Watanabe, and H. Inoue, *Optics Express* **11**(20), 2549 (2003).
- [4] C. Jagadish, H. H. Tan, A. Krotkus, S. Marcinkevicius, K. P. Korona, and M. Kaminska, *Appl. Phys. Lett.* **68**(16), 2225 (1996).
- [5] P. Polynkin, A. Polynkin, M. Mansuripur, J. Moloney, and N. Peyghambarian, *Optics Letters* **30**(20), 2745 (2005).
- [6] A. S. Weling, B. B. Hu, N. M. Froberg, and D. H. Auston, *Appl. Phys. Lett.* **64**(2), 137 (1994).
- [7] A. S. Weling and D. H. Auston, *Journal of the Optical Society of America B* **13**(12), 2783 (1996).
- [8] T. E. M. Staab, R. M. Nieminen, M. Luysberg et al, *Physica B* 340, p. 293 - 298 (2003).
- [9] D. C. Look, D. C. Walters, G. D. Robinson, J. R. Sizelove, M. G. Mier, and C. E. Stutz, *Journal of Applied Physics* **74**(1), 306 (1993).
- [10] G. Molis, A. Krotkus and V. Vaičaitis, *Appl. Phys Lett.* **94**, 091104 (2009).
- [11] R. Adomavičius et. al., *Appl. Phys. Lett.* **85**, 2463-2465 (2004).
- [12] M. Reid, I. V. Cravetchi and R. Fedosejevs, *Phys. Rev. B*, **72**, 035201 (2005).
- [13] G. H. Glover, *J. Appl. Phys.*, **44**, 1295-1301 (1973).
- [14] P. A. Rolland et. al., *Electron. Lett.* **15**(13), 373-374 (1979).
- [15] H. L. Hartnagel, R. Katilius, and A. Matulionis, *Microwave Noise in Semiconductor Devices* (Wiley, New York, 2001), p. 146.
- [16] J. K. Luo, H. Thomas, D. V. Morgan, and D. Westwood, *Journal of Applied Physics* **79**(7), 3622 (1996).
- [17] A. S. Weling and D. H. Auston, *Journal of the Optical Society of America B* **13**(12), 2783 (1996).
- [18] J. Stigwall, A. Wiberg, *IEEE Photonics Technology Letters* 19 (2007) 931.

- 
- [19] A. Rühl, *The Normal Dispersion Regime In Passively Mode-locked fiber oscillators*, Cuvillier Verlag, Göttingen (2008).
- [20] G.P. Agrawal, *Applications of Nonlinear Fiber Optics*, Academic Press, San Diego, 2001.
- [21] A. E. Siegman, *Lasers*, University Science Books, (1986). pp. 105–108.
- [22] Zhiping Jiang and Xi-Cheng Zhang, *IEEE Trans. Microwave Theory Techn.* **47**(12), 2644 (1999).
- [23] V. Pačebutas et. al., *Appl. Phys. Lett.* **97**, 031111 (2010).
- [24] I. Kašalynas et al., *Proc. of the 38th Internat. Conf. on Infrared, Millimeter and Terahertz Waves IRMMW-THz 2013, Mainz on the Rhine, Germany, September 1st–6th (2013) pp. Mo 8-5.*